Master's Thesis of Landscape Architecture

Estimation of Mean Radiant Temperature in urban canyons using Google Street View

구글 스트릿뷰를 이용한 도시 협곡 내 평균복사온도 추정

February 2021

Graduate School of Seoul National University
Department of Landscape Architecture and Rural Systems Engineering, Landscape Architecture Major

Eun Sub Kim

Estimation of Mean Radiant Temperature in urban canyons using Google Street View

Under the direction of Adviser, Prof. Dong Kun Lee

Submitting a master's thesis of Landscape Architecture

February 2021

Graduate School of Seoul National University
Department of Landscape Architecture and Rural Systems Engineering, Landscape Architecture Major

Eun Sub Kim

Confirming the master's thesis written by
Eun Sub Kim

February 2021

Chair Youngryel Ryu (Seal)
Vice Chair Dong Kun Lee (Seal)
Examiner Jungsuk Kang (Seal)

Abstract

This paper presents a method for estimating Mean Radiant Temperature (MRT) of street canyons using Google Street View (GSV) images and investigates its spatial patterns in street-level on large scale. We used image segmentation using deep learning, project panorama to fisheye image and sun path algorithms to estimate MRT using GSV.

Verification of proposed method can be explained by total of 7 field measurements in clear-sky of street-level, since the estimated shortwave and longwave radiation of value is 0.97, 0.77 respectively. The method proposed in this study is suitable for actual complex urban environment consisting of buildings, tree and streets. Additionally, we compared calculated MRT and LST (Land Surface Temperature) from Landsat 8 in a city scale.

As a result of investigating spatial patterns of MRT in Seoul, We found that Higher MRT of street canyons (>59.4℃) is mainly distributed in open space areas and compact low-rise density building where SVF (Sky View Factor) is 0.6-1.0 and BVF(Building View Factor) is 0.35-0.5, or West-East orientation street canyons with SVF(0.3-0.55). On the other hand, high density building (BVF is 0.4-0.6) or high density tree areas (TVF (Tree View Factor) is 0.6-0.99) showed Low MRT (< 47.6). The mapped MRT results had similar spatial distribution with LST, but the MRT(?) lower (?) than LST in low tree density or low-rise high-density building areas.

And it will help decision makers how to improve thermal comfort at the street-level.

Keyword : Solar radiation, Mean Radiant Temperature, Google Street View, Deep Learning, Thermal comfort, Human Health

Student Number : 2019-20217

Table of Contents

`

List of Figures

List of Tables

Chapter 1. Introduction

1.1. Study Background

Exposure to heat may cause severe illnesses and deaths during intense heat events, especially in large urban areas due to the altered urban climate conditions (Dousset et al., 2011; Gabriel & Endlicher, 2011). As future scenarios of heat-related diseases and mortality become a major public health issue, more higher spatiotemporal assessment of heat stress in cities is needed. Accordingly, in the previous paper, Satellite images were used to retrieve the Land Surface Temperature(LST) in large areas, the data evaluated urban thermal environment and understand the relationship between microclimate condition and human health related heat stress or urban geometry (Y. C. Chen, Chen, Matzarakis, Liu, & Lin, 2016; Eckstein, Künzel, Schäfer, & Winges, 2020; Tran et al., 2020; Yu, Liu, Wu, & Lin, 2009). However satellite is not so useful to estimate heat stress in local areas, since higher spatial resolution, obstacles such as clouds, cost and finer temporal resolution remain significant limitations(Rodriguez et al. 2020).

Otherwise The Mean Radiant Temperature(MRT) is the effective heat related health impact indicator in urban environment(S.Thorsson, J.Rocklov, J.Konarska, F.Lindberg, B.Holmer, B.Dousset, 2014). and MRT estimated using GSV is possible to quantitatively evaluate the amount of heat received by urban environment in the city at point

location. Previous studies proved that there is a high correlation between heat-related diseases or heat stress and MRT, but the calculation formula is complex and difficult to evaluate in city scale. Therefore we need to develop a method that can estimate the exact mrt with a simplified equation in the city scale because MRT is one of the most important human bio-meteorological variables for daytime in no cloud days(Park et al., 2018; Rohat, Flacke, Dosio, Dao, & van Maarseveen, 2019). In previous studies, many models developed to evaluate mean radiant temperature in urban canyons using software and simulation model. For example,(Perini, Chokhachian, Dong, & Auer, 2017) increased nighttime outdoor thermal comfort accuracy by incorporating ENVI-met and TRNSYS(Transient Systems Simulation). (L. Chen, Yu, Yang, & Mayer, 2016) evaluated the MRT of Shanghai city during the summer period using the geographic information system(GIS) based simulation approach using the SOLWEIG model for 3d space construction. (Chow, Fung, & Li, 2014; Matzarakis, Rutz, & Mayer, 2010) calculated the radiant flux and shadow spaces using weather data and other input data at the point of location to estimate MRT. In particular, the MRT value for all-sky can be derived using the formula proposed by (Jendrltzky et al. 1990; VDI 1994; 2008). However, previously developed models need complicated input data such as sky view factor(SVF) and radiative data such as solar radiation fluxes to evaluate at street-level(D. Frohlich, 2013; Krüger, Drach, Emmanuel, & Corbella, 2013).

Recently, Google Street View(GSV), which is publicly and freely accessible data, developed method that can estimate solar radiation in the street-level. (1)(Gong et al., 2018; Li et al., 2017) proposed a method to accurately estimate the SVF required to derive the amount of solar radiation received at the point by converting the panorama image into a fisheye image. (2) (Cândido, Steinmetz-Wood, Morency, & Kestens, 2018; Liang et al., 2020) used deep learning to segment images, and extracted urban morphology factors such as greenness, Tree View Factor(TVF) and Building View Factor(BVF). (3) (Gong, Zeng, Ng, & Norford, 2019) evaluated solar irradiance in street canyons with characterizing the street morphology using diurnal solar path algorithm. Since the proposed methods captured solar irradiance in urban canyons only with GSV images, They can be the useful tool for estimating the MRT.

Therefore, we propose an unique method using the street geometrics characterized with GSV images to quantify the MRT in street-level. The aim of this study is to (1) present MRT estimation method in street-level using Google street view and (2) analyzed difference between LST and MRT in the city scale. In detail, we confirmed that which regions do we appear different in and what factor(urban morphology or street orientation) caused high difference heat. Finally the MRT estimated method proposed in this study is a simplified calculation equation that is easy to calculate and can reflect high resolution and fine temporal range. This can be analyzed more precisely with heat-related health, and can be used

as data for sustainable urban space design in consideration of temporal and spatial thermal environments.

1.2. Literature review

1.2.1 Mean radiant temperature formula

Following the MRT calculation suggested by Fanger (1972), shortwave and longwave radiation fluxes have to be weighted with their respective angle factors and summarise to determine the energy amounts reaching the human body.

$$S_{str} = a_l \times \sum_{i=1}^{n} F_i \times E_i + a_k \times \sum_{i=1}^{n} F_i \times D_i + a_k \times f_p \times I^{\times} \left[\frac{W}{m^2}\right] \quad (1)$$

$$T_{mrt} = \sqrt[4]{\frac{S_{str}}{\varepsilon_p \times \sigma}}[K] \quad (2)$$

The most important advantage of this method is the capability to separate measure of the shortwave and longwave radiation fields, which allows taking into account the different absorption coefficients and the consequent different importance in the radiation energy budget.

A second method of measuring the MRT is based on the utilisation of a globe thermometer.

$$T_{mrt} = \sqrt[4]{(T_g + 273.15)^4 + \frac{h_{cg}}{\varepsilon * d_g^{0.4}} \times (T_g - T_a)} \text{ [K]} \quad (3)$$

In outdoor environments, where the radiant environment

constantly varies in not homogeneous conditions, the globe thermometer is less suitable than the pyranometer/pyrgeometer measurements. Some of the main issues are recognized in the difficulties to approximate the standing position of the human body due to its spherical shape, the impossibility to take into account the different longwave and shortwave radiations absorption coefficients, and uncertainty results due to its long time in reaching the equilibrium in outdoor conditions (Kantor et al., 2011; Thorsson et al., 2007).

According to prior research reviews, mean radiant temperature was evaluated based on the absorption rate of heat energy emitted from urban environmental factors around the that point. For example, ENVI-met simulates the surface-plant-air interactions in an urban environment (Bruse, 2004), ENVI-met calculation of MRT is defined by the following equation (Bruse 1999):

$$T_{mrt} = [\frac{1}{\sigma} \times (E_t(z) \times \frac{a_k}{\epsilon_p} \times (D_t(z) + I_t(z)))]^{0.25} \text{ [K]} \quad (4)$$

And Rayman calculates the MRT from the Stefan-Boltzmann radiation law (Matzarakis, 2006):

$$T_{mrt} = \sqrt[4]{\frac{S_{str}}{a_l \times \sigma}} \text{ [K]} \quad (5)$$

1.2.2 Surface temperature simulation model

A preliminary review of what the tools account for when predicting MRT is proposed in (Table. 1). The (table. 1) is organized

according to the factors that influence MRT predictions at the centre point of a human body: the human body radiation exchanges, the shortwave radiation, the longwave radiation, the sky and surfaces View Factors. It is described how different tools model these factors and with what assumptions(Table. 1)

Table 1 Comparison of outdoor variables for calculating mean radiant temperature

	CitySim Pro	**ENVI-met**	**RayMan**	**Ladybug Tools**	**Autodesk CFD**	**SOLWEIG**	**GSV_MRT**
Urban geometric							
Context with various urban environment types	△	△	x	△	○	△	○
Data collection	Auto CAD 3D software	Leonardo 3D software	2D	Rhino 3D software	Autodesk Revit 3D software	Digital Surface Model(DSM) 2.5D	Panorama image
View factor	Ladybug Raytracing (Diva)	Indexed view sphere	Fish-eye photo	Ray Tracing	Numerical Method	Shadow casting algorithm	Image calssification
Human Body Radiation Exchange							
Shortwave absorption	○	○	○	○	△	○	○
Longwave emissivity	○	○	○	○	△	○	○
Shortwave Radiation							
Solar irradiation	Radiosity Algorithm	Empirical equations	Input data	○	○	○	Erbs model
Direct reflected radiation	Radiosity Algorithm	Average albedo	Estimated by solar elevation	△	△	Shadow-casting algorithm	Shadow/ Sunlight
Diffuse reflected radiation (Vegetation)	○	○	△	○	△	○	○
Diffuse reflected radiation (Ground)	○	○	△	△	○	○	○
Longwave Radiation							

Surface Temperature	heat balance equation	Heat exchange model	Simplified Net radiation	Man-Environment Heat Exchange Model	Heat exchange model	Parametetrization for different ground cover	Parametetrization for different ground cover
Longwave exchange with the sky	○	○	○	○	○	○	○
Longwave reflected radiation	○	Average emissivity	Average emissivity	EnergyPlus model	View Factor	Sunlit wall faction	Sunlit wall faction
Longwave radiation (Vegetation)	○	○	△	○	x	○	○
Longwave radiation (Ground)	○	○	△	○	○	○	○
Transpiration (Vegetation)	Input data	Input data	x	x	x	○	x
Calculate MRT	Integral radiation measurement	Integral radiation measurement	Globe-thermometer method	SolarCal model	Finite Element Methods	Integral radiation measurement	Integral radiation measurement

(1) Data collection

In previous studies, 3D model software and DSM data from satellite images are used to analyze heat energy exchange in a 3D space. In case of the 3d model software, urban environmental factors such as trees and buildings can be specifically described to calculate accurate urban thermal energy, whereas decreasing computational efficiency such as cost and time should be limited to build a wide range of cities. On the other hand, construction of 3D data through satellite image e.g DSM, DEM can be efficient in terms of 3d data construction time. but it is difficult to obtain specify the characteristics of the city. Meanwhile in the case of Google Street View, which is easy to acquire data with open source data, The computational time could be save in the data collection and processing big data process. Google street view has the advantage of acquiring spatial information of cities in countries where urban construction data is difficult or there is no urban spatial data.

(2) View factor

The definition of the sky and surface view factors play a crucial role in the determination of the whole radiation field. Here CitySim Pro, ENVI-met and Autodesk CFD are the tools that provide the best accuracy due to their deterministic calculation method. The view factor calculation method based on the above research takes a long time because it calculates all factors that are visible within a 360 degree radius from the point of view. (Nice et al. 2018) shows that the radiosity method. It could be consider objects as obstructions (shadow casting) and offers several time-saving features to shorten the already very fast computation time.

Rayman model uses a Fish-eye photo method to calculate Sky and Surface View Factors. Meanwhile, in the case of GSV, it is possible to classify images accurately of 80% through deep learning, which has the advantage of calculating the View Factor in any area. Especially, when analyzing based on the trained data, the data processing is fast, and all the factors of the city such as concrete, brick, glass in building wall, cement, wood, grassland etc can be extracted. GSV allows us to specifically set the albedo and emission rate required for the radiant energy flux for estimate mean radiant temperature.

(3) Radiation

Depending on the model, the method of calculating the reflected radiation energy is different. In the case of Autodesk CFD, It can be

partition between non-shaded fraction of a building based on the position of the sun. In case of ENVI-met and Ray-man, it is possible to calculate a wide range rapidly to evaluate the solar radiant energy by applying the average albedo in the range and the emission rate. Also, in the case of SOLWEIG, the ratio of the shadowed wall according to the altitude of the sun at the point is derived and calculated. To evaluate solar energy rapidly and simply, Tis study utilized that SOLWEIG method because the long-wave radiation derived from previous studies was accurate, and the proportion of shadows can be calculated in a short time in 3D space.

(4) Surface temperature

Surface temperature is required to calculate the emission wavelength. Citysim pro, ENVI-met, Autodesk CFD constructed the surface temperature through an energy balance model. It can be calculated from air temperature, wind speed, storage heat flux, and net radiation flux. Since there is no input data and the calculation formula is complicated, Offerle and Grimmond (2003) derived an equation using Ta, which is the near-surface temperature (person level), and in the case of SOLWEIG, the empirical equation for Parametetrization for different ground cover. The surface temperature was estimated through. Calculate the relationship between Solar elevation and Ts-Ta to analyze the relationship between time and shadowed and non-shadowed surfaces, and multiply the shadow ratio derived above to calculate long-wave radiation. (Huang 2012, Janicke et al., 2016) analyzed the

relationship between the surface temperature and the air temperature through actual measurements, and as a result, the average air temperature and the surface temperature were the same. , Buildings, roads, etc.) and air temperature were analyzed to create a regression model.

Chapter 2. Study area and data

2.1. Study area

Seoul is one of the largest and densely-populated cities in the world. The city with a population about 9.8 million living in around 606 square kilometers of developed land. Situated at the west of the central part of Korea with basin surrounded by mountains, Seoul is cold under the influence of the dry continental high pressure in winter and hot and humid in the summer under the influence of high temperature and humidity in the north pacific ocean(Fig.1). Heat stress is increasing due to the increase in high-density skyscrapers due to the recent overcrowded urbanization. In addition, Seoul is a metropolitan area with the highest population density among OECD member countries (Korea Institute of Land, Infrastructure and Transport, 2015), and the elderly population accounts for 9.3% of the total population. Seoul has experienced rapid urbanization with high-density building and associated urban heat island (UHI) effects. UHI would significantly affect the disease related heat stress living conditions. In addition Seoul is a large city with the highest population density among OECD member countries (Korea Research Institute of

Land, Infrastructure and Transport, 2015), and the elderly population accounts for 9.3% of the total population. Therefore The number of vulnerable populations is predicted to increase due to the continued rise in the elderly population ratio and urbanization. In this paper, Seoul was selected as a representative area to improve the thermal environment, and temporal/spatial MRT was evaluated using GSV panorama images.

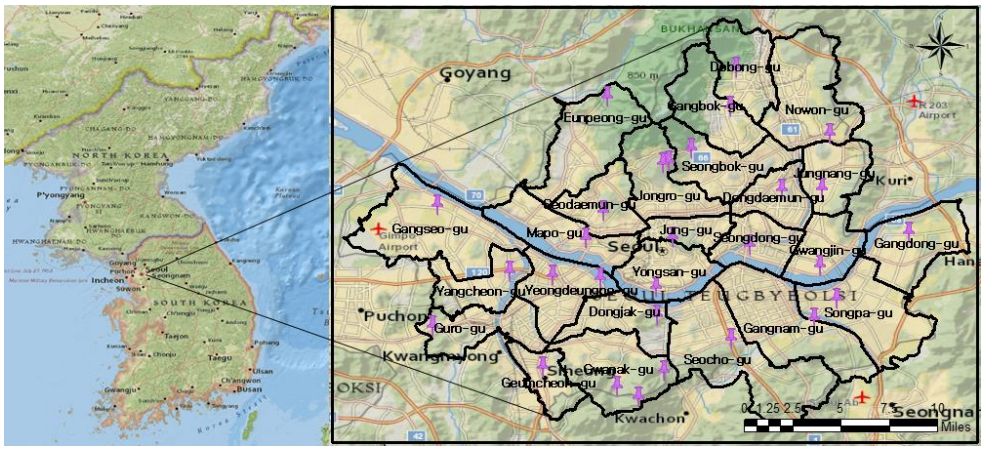

Figure 1 Location of the study area (City of Seoul). The total area is about 605.21 km 2 and the population of the city is 9.8 million.

2.2. Data collection

we collected two data(Google Street View image, landsat8 satellite image) for estimating MRT and comparison between LST and MRT (Table. 2). At first, We collected total 344,044 street panorama images sampled using the GSV Application Programming Interface(API) at 30-m intervals in the high-density urban area of Seoul. And in order to compare with the seasonal LST, GSV was collected by classifying season based on the time when trees fell. To

derive solar path in fisheye image of street canyon, we adjusted to the north by shifting the vehicle heading direction (Gong et al., 2019). we also collected air temperature, humidity, direct solar radiation, long wave radiation using net radiometers CNR4 (Kipp & Zonen, 2008), 175H1 equipment for validating our method. Climate data required for mrt estimated(air temperature, humidity) were collected from (https://data.kma.go.kr)

Finally we collected landsat 8 OLI/TIRS C2 L2 image To analysis difference between LST and MRT. Two Landsat 8 OLI/TIRS images covering Seoul with less than 10% cloud cover are selected. For the Landsat 8 data, Band 4, 5 and 10 were used for derivation of Land Surface Temperature(LST). The Landsat8 data set is currently available free of charge from the USGS website (https://earthexplorer.usgs.gov).

Table 2 Study area for verification and application in each 2018, 15.10. 2020. Latitude (Lat) and Longitude (Log) were used for collecting GSV panorama images (GSV_pano).

	Object	Location	Lat	Log	Data	Num of panorama
Google Street View	Validation sites	Low building	37.457391	126.948493	Radiation (shortwave, longwave), air temperature, relative humidity	7
		Park	37.495193	127.003546		
		Commercial area	37.521532	126.927314		
		Apartment	37.503094	126.943548		
		River	37.528474	126.934370		
		Narrow	37.482026	126.92		

		alley		9579		
		Residential area	37.469727	126.942584		
			Summer (6 ~ 10)		Air temperature	58,794
	Mapping	Seoul	Winter (12 ~ 3)		Relative humidity	285,243

	Atrribute					
	Date	Satellite image	Projection/Datum	Cloud cover	Sensor	Time
Satellite image	2018. 06. 19	Landsat 8	UTM zone52/ WGS84	1.79	OLI_TIRS	09:52
	2018. 12. 19	Landsat 8	UTM zone52/ WGS84	1.20	OLI_TIRS	10:39

Chapter 3. Method

3.1. Research flow

This study presents an estimation method Mean Radiant Temperature(MRT) using Google Street View in high density urban area and and analyzes comparison between LST and MRT in city scale. In order to accurately estimate the MRT, VF and surface temperature must be accurately calculated (Appendix. 3). However estimating the View Factor and surface temperature each urban materials in complex urban geometry is difficult. At first we implemented using the scene parsing method in a deep-learning frame work [Gong et al., 2019], as shown in (Fig.4) and then We calculated the long-wave radiation by using the rate which short-wave radiation is absorbed by the urban surface based on the measured data (Offerle & Grimmond. 2003; Ulden & Holtslag. 1983).

In order to verify the accuracy of the method presented in this study, we compared with the measured data of 7 times. Finally We performed a comparative analysis between mrt and lst in Seoul based on the method presented in this study. (Fig. 2) presents a complete flow chart

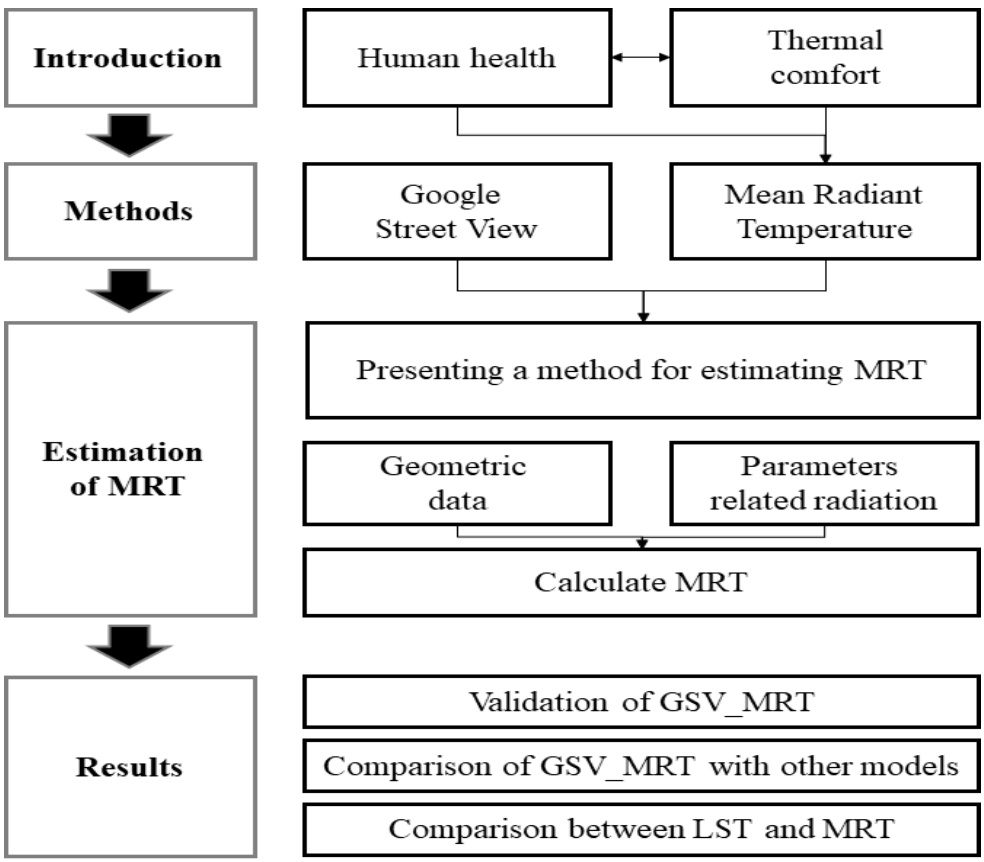

Figure 2 Flowchart of our research process

3.2. MRT simulation

3.2.1. Schematic flow for MRT simulation

The MRT simulation method suggested in this study is presented in (Fig. 3). It consists of three main phases. In phase I (blue

rectangles), we built input data. Urban structures such as sky, tree, and building are extracted based on the deep learning image classification method,. The classified images are used for calculating the VF (section 2.3). We built fisheye images from the Panorama images to estimate SVF and used Sun path algorithm by checking the shadow status(Gong et al., 2019; Reda & Nrel, 2005). Phase II is the radiation calculation process (green rectangle). We calculated shortwave and long wave radiation for MRT calculation in street-level under the clear sky. Solar radiation was calculated for each VF(SVF, TVF, BVF, RVF SiVF) estimated in the above step, and outgoing long wave radiation was derived from the result of 50-year measurement data of(Holtslag & Van Ulden, 1983; Loridan et al., 2011; MOTRON L. BARAD, 1958) .We combined the street morphologies and the solar path from (Phase I) to derive the clear-sky street-level solar radiance; In Phase III (yellow rectangle), we estimated the MRT using the incoming shortwave and longwave

radiation.

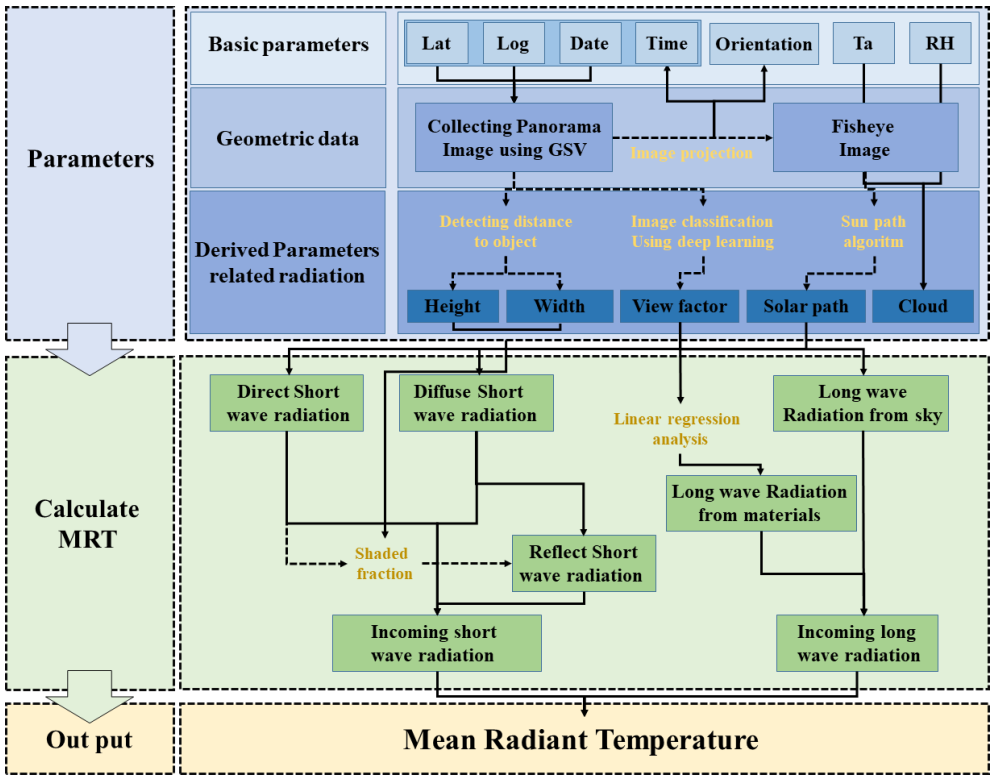

3.2.2. Urban canyon geometry calculation using GSV images (Phase I: built geometry data)

In this section, we introduce how to use GSV images to calculate the view factors of street canyons and sun path in fisheye image in street-level. . The workflow procedure is shown in (Fig. 4). First, images were classified using the scene parsing method in a deep learning based on previous research(Brostow, Fauqueur, & Cipolla, 2009; L. C. Chen, Zhu, Papandreou, Schroff, & Adam, 2018). The

Figure 3 Schematic flow for calculating MRT using GSV

view factor for each urban element(building, tree, side-walk and

road) was calculated using the deep learning(PSPnet) to segment image (Liang et al., 2020). Here surface albedo, Absorption coefficient and heating coefficient were assigned in (Table. 3).

We project the panorama images from cylindrical to azimuthal projection to generate the fisheye images, as shown in (Fig. 4) using (Gong et al., 2019)method. The solar zenith and azimuth angle were calculated by using date, time and location information of collected panorama images to calculate the sun path. Last, the shadow was calculated by overlaying the sun path coordinates on the fisheye image.

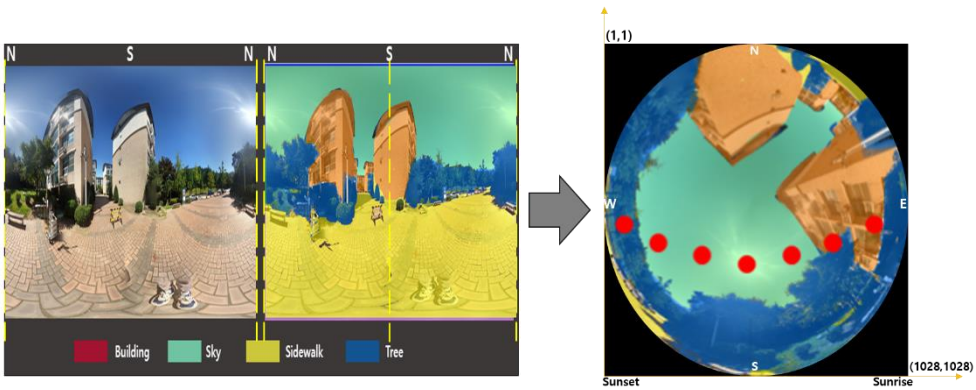

Figure 4 Workflow procedure for image segmentation to calculate VF using PSPnet. And convert panorama image to fisheye image with solar path algorithm to calculate short direct radiation.

Table 3 Materials table about absorption coefficient, albedo, heating coefficient.

Material	Absorption coefficient	Albedo	Heating coefficient
Building	0.6	0.4	0.08

Pavement	0.86	0.14	0.08
Sidewalk	0.7	0.3	0.08
Tree	0.85	0.15	0.25
Grass	0.75	0.25	0.12
Soil	0.7	0.3	0.38

3.2.3. Street canyon solar radiation calculation (Phase II:radiation transfer calculation.)

3.2.3.1 Calculation of street-level shortwave radiation

To calculate clear sky short wave radiation, we used the fraction of cloud cover and figured how the extraterrestrial radiation changed due to cloud amount as it enters the atmosphere (Allen, Pereira, Raes, & Smith, 1998) (Eq. 1)

$$I_g = 0.75R_a(1 - 0.75^{FCLD})^{3.4} \quad (1)$$

Here I_g is clear-sky solar radiation(MJ $m^{-2}day^{-1}$), R_a is extraterrestrial radiation and FCLD is fraction of cloud cover. We separated Direct radiation(S_{dir}) and Diffuse radiation(S_{diff}) using the Cloud Radiation Model(CRM) developed by (KAHRAMAN, 2016; Kasten & Czeplak, 1980) to obtain a better assumption under more complex conditions.

$$S_{diff} = I_g(0.3 + 0.7 \times FCLD^2) \quad (2)$$

$$S_{dir} = I_g - S_{diff} \quad (3)$$

Here S_{dir} and S_{diff}mean direct short-wave radiation and diffuse short-wave radiation . The (eq. 1) that can reflect the shadow can be derived short-wave radiation from the daily actual duration of sunlight over hours per day. According to the Meteorological Administration, the altitude in Seoul, Korea densely populated area is 15 to 60 m, and if this is substituted for the station elevation above sea level, the value of 0.7503 to 0.7512 is obtained. Also, if you substitute 200m, which is the height of high-rise buildings, the value is0.754. Therefore, the value of 0.75 in the formula (eq. 1) can be estimated by considering shadow radiation in urban areas with high dense buildings. We calculated incoming direct incident (S_{dir}), scattering (S_{diff}), and reflected shortwave radiation ($S_{reflect}$). Was calculated through the following equation:

$$S_{dir\downarrow} = S_{dir} \times f \quad (4)$$

$$S_{diff\downarrow} = S_{diff} \times \Psi_{sky} \quad (5)$$

$$D_{reflect\downarrow} = \sum_{n=1}^{k}(D_{dir} + D_{diff}) \times a \quad \times VF_n \times f \quad (6)$$

Here, f is expressed as binary according to the presence or absence of a shadow at the measurement point. If f equals zero ray path is masked by an obstacle. K is the number of materials of the classified image, and in this study, it was set to 6, and a means albedo for each material.

3.2.3.2 Calculation of street-level long-wave radiation

In case of the long-wave radiation, three types of longwave radiation were calculateded: (1) The incoming long-wave radiation from the atmosphere($L_{\downarrow}$), emitted long-wave radiation from the urban elements($L_{\rightarrow}$) and outcoming long-wave radiation($L_{\uparrow}$) were calculated using NARP model proposed by (Loridan et al., 2011; Offerle, Grimmond, & Oke, 2003). The NARP model calculates the long-wave radiation by considering the amount of water vapor in the atmosphere and the amount of cloud (Eq. 7) note that the longwave radiation process more specific than the previously proposed(Allen et al., 1998).

$$L_{\downarrow} = (\epsilon_{clear} + (1 - \epsilon_{clear})FCLD)\sigma T^4 \quad (7)$$

Incoming long-wave radiation from urban elements in urban canyons (L_{sky}) is calculated using SVF estimated from fisheye images (Eq. 8).

$$L_{sky} = L \times \Psi_{sky} \quad (8)$$

Emitted long-wave radiation from the urban elements is calculated from all VFs except SVF using the long-wave radiation conversion ratio (we regarded it as a heating coefficient, table. 3). In order to accurately estimate the long-wave radiation, the surface temperature have to be calculated using an energy balance model. But (Holtslag & van Ulden. 1983) calculated by using the constant value of shortwave radiation that affects the surface temperature. Although the conversion ratio of shortwave radiation shows high

accuracy on a clear day, decreases rapidly after sunset (Night time). However, at night, the stored heat is released and the difference between the air temperature and the surface temperature is insignificant, so the error is low in areas(high density building or compact area. Therefore, in this study, the amount of emitted long-wave radiation was calculated using the following equation using the ratio (fsw) at which the absorbed long-wave radiation is converted to long-wave radiation(Offerle & Grimmond. 2003; Ulden & Holtslag. 1983).

$$L_{\uparrow} = \sigma T^4 + fsw\left(S_{dir} + S_{diff}\right) \times (1 - a) \quad (10)$$

Outgoing longwave radiation is the amount of radiation emitted from storage heat surfaces by the amount of short wave radiation, and was calculated using the heating coefficient and albedo.

In previous studies, the value of fsw was different depending on the land use.(grassland : 0.12, bare : 0.38, impermeable surface : 0.08) (Ulden & Holtslag' s. 1983; Barad et al., 1958; Ulden, Holtslag. 1983; Offerle & Grimmond. 1983) However, in previous studies, there is no study using the fsw of individual factors such as buildings and trees. In this study, the fsw was derived based on the measured data and then outcoming long wave radiation was calculated using the following equation.

$$L_{\downarrow} = \mathrm{Ldw} \times \mathrm{SVF} + \sum_{i=1}^{n} VF_{(i)} \times (\mathrm{Ldw} + fsw_{(i)} \times \left(S_{dir} + S_{diff}\right) \times \left(1 - a_{(i)}\right) + VF_{(i)} \times (1 - E_{(i)}) \times Ldw \quad (9)$$

As a result of deriving the fsw by considering the ratio of albedo

for each factor, the value of Building:0.19 Tree:0.3 was derived.

3.2.4. Phase III mean radiation temperature calculation

MRT is calculated from the radiation of the urban elements surrounding a pedestrian. (Jamei & Rajagopalan, 2017). This study includes building, pavement, sidewalk, tree, grass, and soil for the urban elements. These elements reflect direct- and diffuse-shortwave radiation and emit and reflect longwave radiation, which are summed using Eq. 11 (D. Frohlich, 2013; Matzarakis et al., 2010). a_k is the absorption coefficient, and ε is the emissivity of the pedestrian, which has standard values of 0.7 and 0.97 (Lindberg & Grimmond, 2011).

$$T_{mrt} = \left(\frac{1}{\sigma} \sum_{i=1}^{n} (E_i + a_k \frac{D_i}{\epsilon_p}) \right)^{0.25} - 273.15 \quad (11)$$

Chapter 4. Result and Discussion

4.1. verification of solar radiation estimated in street-level

In this section, the developed GSV-based solar radiation estimation method is evaluated using field measurements in street-level (Fig. 5). Further, The difference in the accuracy of validation sites was compared from total of 7 sites (table. 4). (Appendix. 1) shows the validation between the measured data and the estimated shortwave and longwave radiation. As a result, on the whole, a consistent variation trend can be observed. The estimated shortwave

radiation was estimated to be slightly higher overall than the measured data. The differences between calculated and measured Shortwave radiation from -19 to +23 W/m^2 during daytime.

It seems that reason for this is because the patterns of anthropogenic energy usage, which decrease in storage efficiency at high wind speed and estimated SVF based on GSV. However, the (Appendix. 1) shows that the shadow detection using the sun path algorithm is well captured from the changing short-wave radiation. In the case of the comparison between the estimated long-wave radiation and the measured data, it can be seen that the difference is larger than that of the short-wave radiation. (Appendix. 2) shows that the difference between outcoming longwave radiation is -20 W/m^2 and +50 W/m^2, respectively during 12-14pm. and incoming longwave radiation show that underestimates during sunset time. The cause of the overestimation and underestimation of long-wave radiation is due to inaccurate surface temperature. We are overestimated in sites with many impermeable surfaces such as buildings, sidewalks, pavements, otherwise underestimated in sites with a high percentage of green space. For accurate long-wave radiation estimation, we need to measure the Fsw ratio in point of location where we want to estimate.

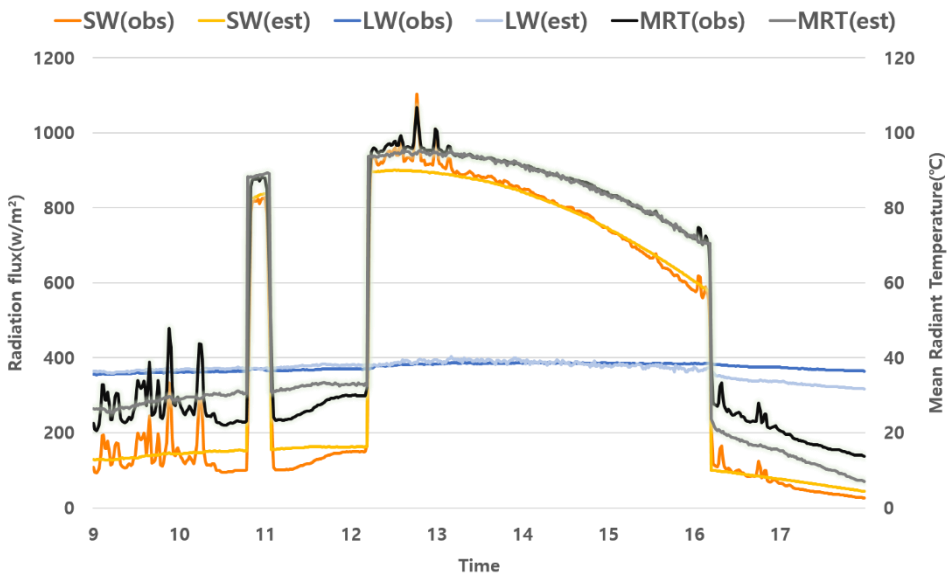

Figure 5 Comparison between estimated shortwave, longwave radiation, MRT and data measured in korea over hourly. (orange, yellow line) is incoming shortwave radiation, (blue line) is incoming longwave radiation, (black,gray line) is mean radiant tempera

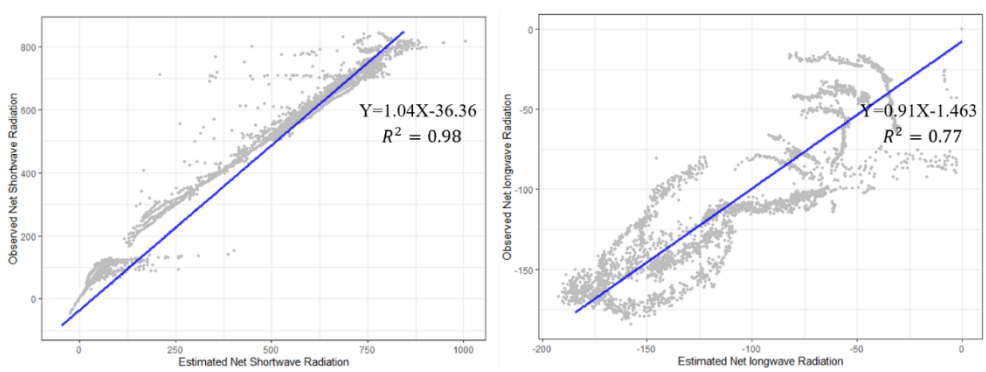

Figure 6 Validation of Short-wave radiation(R^2 =0.98) AND Long-wave radiation(R^2=0.77)

The method proposed in this study for estimating shortwave and longwave radiation was generally shown similar trends. this gave satisfactory results for estimating solar radiation($R^2 = 0.97, R^2 = 0.77$)(Fig. 6). In particular, long-wave radiation estimated by using the ratio method of converting short-wave radiation to long-wave

radiation has a great influence on short-wave radiation. Although there was a difference between the measured data values, it is of great significance that it shows similar trend despite the use of a simple formula. Therefore we can conclude that the spatial pattern of the solar radiation in street level can be predicted by the developed GSV-based method.

4.2. Validation of Long-wave radiation

(Fig. 7) shows the comparison between the measured data and the estimated long-wave radiation between measurement sites during the day. The higher the SVF, portion of the sky covered by clouds and composed of a single surface element(Low building Park, River) is overestimated. On the other hand, sites with low SVF and complex urban structures are underestimated at night. For example, in Commercial area, Narrow alley, Residential area, there is a difference of about(-48W/m2, -31W/m2, -31w/m2) between the measured data.

We can confirm that (Fig. 7) is related to the negative correlation between albedo and long- wave radiation. In addition, when the albedo value changes dramatically, the difference between the measured data appeared. Therefore, we can more accurately estimate the long-wave radiation when considering the albedo value that changes with the altitude of the sun.

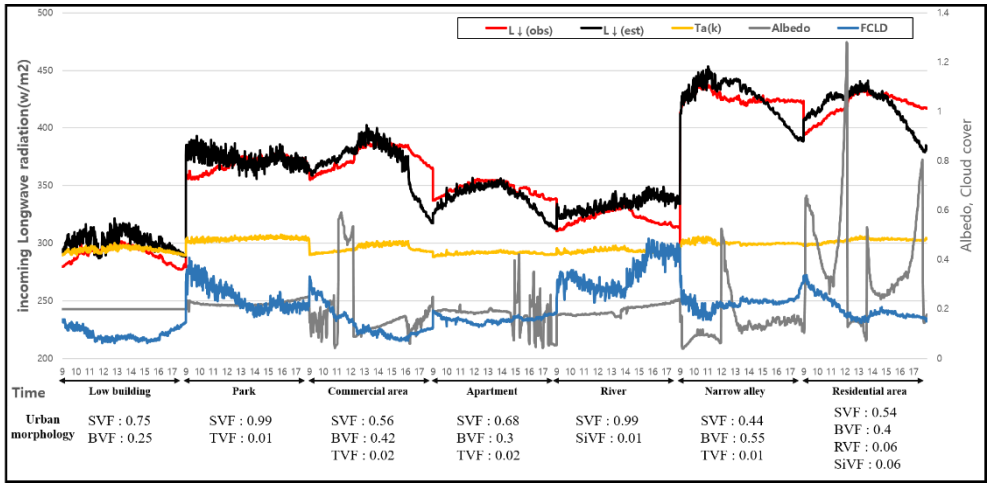

Figure 7 Analysis of Incoming long-wave radiation by comparison with meteorology data, albedo and urban morphology from 7 sites. Amount of cloud was calculated using Ta and RH.

4.3. Comparison between LST and MRT estimated using GSV

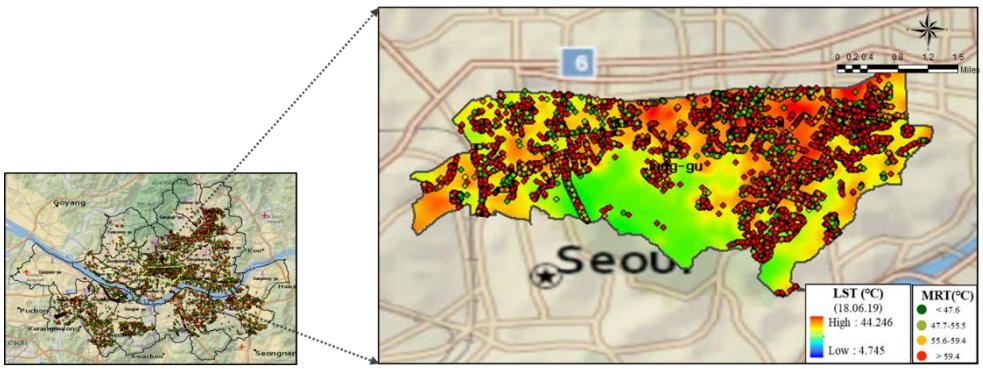

Figure 8 Comparison mapping with MRT and LST in Jung-gu, Seoul. Point data means MRT estimated in paper. But there is no data on the green area because the point data was evaluated based on the street. The data mapped to the surface was LST that landsat data on

We confirmed (1) solar radiation under the effect of street morphologies and urban geometries at 10:00am with LST and (2) classified regions with high or low MRT Based on comparative analysis between LST and MRT. We assumed clear-sky to analyze the effect of solar radiation according to the street canyons and used only GSV data acquired during the summer period. Because leaves fall in other seasons, and cause an error in TVF value (Fig. 8).

As a result of LST analysis in Seoul, it was found to be high (about 29℃ ~ 35℃) in area with no obstacles and a large impervious surface such as compact low-rise density building, compact mid-rise density building and external parking lot (about 29℃ ~ 35℃). And low LST was distributed in the permeable surface (dense tree, low plants) and high density building area (about 17℃ ~ 26℃) (Fig. 9). Similarly higher MRT of street canyons (>59.4℃) is mainly

distributed in open space areas(low plants, bare paved area) and compact low-rise density building (SVF, BVF are around 0.6-1.0, 0.35-0.5) or street canyons with West-East orientation(SVFs are around 0.3-0.55)(Table. 4). The main cause of high MRT values in low plants with low LST is SVF. Otherwise Lower MRT of street canyons(<47.6℃) is mainly distributed in high building(compact mid-rise density building and high density building) or tree coverage areas (BVF, TVF are around 0.4-0.6, 0.6-0.99)(Fig. 9). In particular, in the compact low-rise density building area, LST is high. But low SVF and high BVF with high H/W ratio has low MRT(Table. 4). Therefore, since the results of thermal stress analysis through LCZ classification differ results between Urban geometries and MRT, heat as well as temperature must be considered in thermal vulnerability analysis or health impact analysis (Kwok et al., 2019; Zhou et al., 2020).

From this result, we can confirm three characteristics. (1) TVF has a negative relationship with SVF, and the difference in the direct shortwave radiation indicates significantly depending on the presence or absence of a shadow (about 421w/). (2) streets with West-East orientation receive higher solar radiation than other street orientation. because it becomes horizontal with the path of the sun and decreases shade area. (3) Compact mid-rise density building areas with low SVF and high BVF have high LST and low MRT, but low plants have low LST and high MRT.

Table 4 Point location data for comparative analysis between LST and MRT. We focused urban morphology and street orientation to analyze in which regions the MRT-LST difference is significant.

	urban morphology	Location	Latitude	longitude	Land Surface Temperature	SVF	TVF	BVF	Street orientation	MRT
High LST	caompact low-rise density building	205-422, Cheongnyangni-dong, Dongdaemun-gu	37.5895	127.0414	31.627	0.75	0	0.25	N-S	
		Anam-ro 24-gil, Jegi-dong, Dongdaemun-gu	37.5882	127.0362	33.015	0.64	0.01	0.35	E-W	
		Changsin 1-dong, Jongno-gu	37.5718	127.0139	32.141	0.41	0	0.59	N-S	
		977-18, Bangbae-dong, Seocho-gu	37.4815	126.9923	32.542	0.6	0.02	0.38	E-W	
		Munrae-dong 4-ga, Yeongdeungpo-gu	37.5147	126.8906	33.771	0.7	0	0.3	E-W	
	bare paved area	Suseo station parking lot	37.4854	127.1056	34.783	-				
		735, Suseo-dong, Gangnam-gu	37.4878	127.0998	35.232					
		Ilwonbon-dong, Gangnam-gu	37.4874	127.0801	35.547					
	compact mid-rise density building	279-47 Sangdo 4-dong, Dongjak-gu	37.4957	126.9374	29.341	0.42	0	0.58	NE-SW	
		41-5, Hwayang-dong, Gwangjin-gu	37.5451	127.0666	29.997	0.38	0	0.62	N-S	
		254-239, Daehak-dong, Gwanak-gu	37.4649	126.9359	31.011	0.3	0	0.7	E-W	
		9-34, Suyu3-dong, Gangbuk-gu	37.6383	127.0205	30.014	0.55	0	0.45	E-W	
Low LST	Dense tree	Nakseongdae park	37.4719	126.9599	18.354	0.03	0.97	0	E-W	
		Janggunbong Sports Park	37.4787	126.9384	18.997	0.01	0.99	0	E-W	
		44-3 Ogeum-dong, Songpa-gu	37.5051	127.1277	19.584	0.3	0.6	0.1	NE-SW	
	low plants	Montmartre park	37.4954	127.0038	21.711	0.99	0	0..01	NE-SW	
		Yeouido hangang park	37.5293	126.9326	22.667	0.96	0	0.04	N-S	
		pyeonghwaui park	37.5618	126.8907	23.421	0.95	0	0.05	E-S	
	High density building	460 Hongje-dong, Seodaemun-gu	37.5854	126.9506	24.145	0.55	0.03	0.42	E-W	
		140 Garak-dong, Songpa-gu	37.4956	127.1278	25.245	0.4	0	0.6	N-S	
		467-7 Dogok-dong, Gangnam-gu	37.4882	127.0519	26.114	0.42	0.21	0.37	N-S	
		27-45 Sangdo 2-dong, Dongjak-gu	37.5043	126.9433	25.773	0.52	0.02	0.46	E-W	

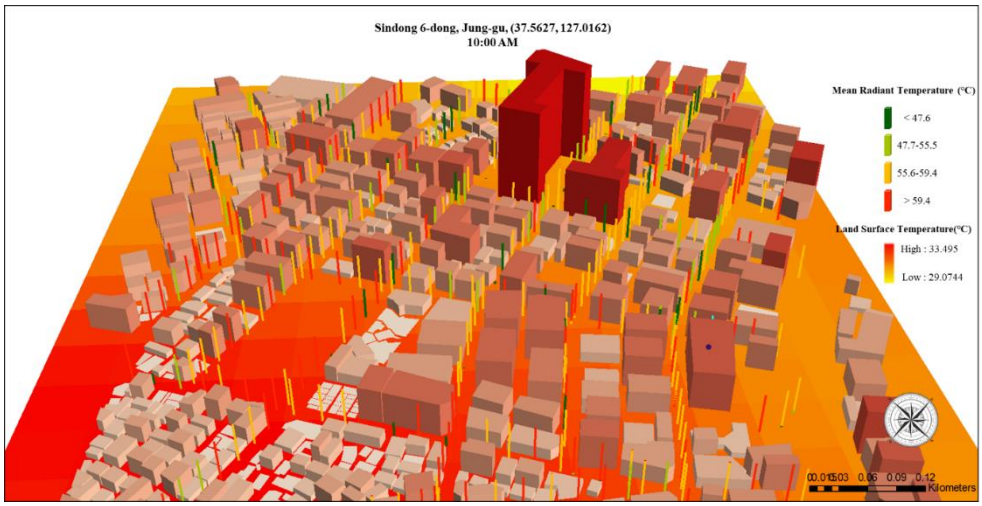

Figure 9 Comparison analysis between Land Surface Temperature and Mean Radiant Temperature at Sindong 6-dong, Jung-gu, Seoul which had a compact high and mid-density building. Bar graph mean MRT. We classified the MRT value into 4 classes based on the analysis result between MRT and heat risk in the previous(S.Thorsson, J.Rocklov, J.Konarska, F.Lindberg, B.Holmer, B.Dousset, 2014). And surface mean LST using Landsat 8 image.

4.4. Comparison of GSV_MRT with other models

The comparison was focused on the SOLWEIG, ENVI-met, and Rayman models that are widely used in previous studies (Matzarakis, 2017; naboni et al., 2020). Based on the RMSE and index of agreement values (5.02° C, 4.25° C and 0.97, respectively), The MRT estimation method using GSV was more accurate than other models (Gál & Kántor, 2020). The reason that the difference in short-wave radiation is larger than that of other models is due to the amount of short-wave radiation transmitted through the tree and the error of estimating SVF. However, these factors have an insignificant effect on shortwave radiation. (difference: 0.2w/m^2). Although the method proposed in this paper is overestimated by about (46w/m2)

in shadow time (Fig. 10), tend to overestimate Tmrt during prolonged periods of shade and underestimate when the sites are sunlit, it can be seen that the emitted short-wave radiation is applied as similarly as 3D, since a similar trend appears with other models.

In contrast, long-wave radiation shows the lowest RMSE value among the three models. These results show that the calculation formula using the absorption rate of short-wave radiation can accurately estimate long-wave radiation in clear weather except at night (Offerle et al., 2003). These errors indicate room for improvement with regards to surface temperature estimation and shortwave reflected radiation calculations in the models, because there is a rapid change depending on short-wave radiation variation

The results of comparison between the three models commonly used to calculate MRT in cities scale and the method presented in this study, The MRT estimated using GSV shows high overall accuracy. In particular, this method can estimate the MRT through a 360-degree panorama image in an area that requires less input data than other models (only temperature, humidity). Therefore This makes it easy to acquire data because it does not use 3D software programs and can construct data by taking 360-degree pictures.

GSV has the advantage of acquiring data from the 2.5D perspective and viewing many objects on one screen, including the point of view. Since 2D models such as single layer and multi-layer are limited to the height of the same building in the horizontal space and cannot take into account a three-dimensional effect, the error is

greater than 2.5D when calculating the view factor in real space. Therefore, MRT evaluation on the 2.5D side has the advantage of being able to evaluate the MRT by three-dimensionally considering the complex urban spatial factors in the horizontal space. Although the accuracy may be lower than that of the 3D model, the results similar to those of the software program evaluating MRT based on the 3D model can be confirmed, and MRT estimated using GSV can be quickly evaluated in cities scale

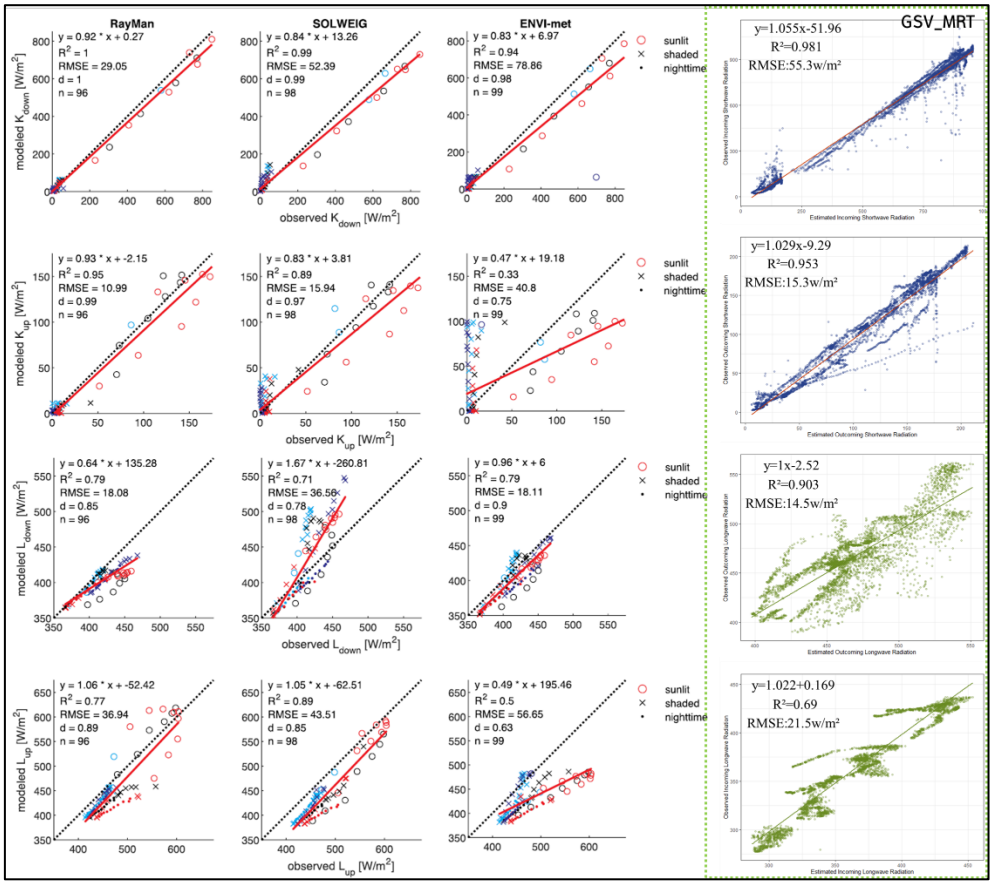

Figure 10 Comparison between shortwave, longwave radiation of other models(Rayman, SOLWEIIG, ENVI-met) and value estimated from google street view

4.5. limitations and future development

Accurate estimation of shade and surface temperature is the most important factor in MRT prediction. Because surface temperature varies depending on the presence or absence of shade. Although We calculated the solar irradiation by considering shaded area ratio using (Allen et al., 1998) method, we need to height data to accurately estimate the proportion of shaded area. Meanwhile, in the field of data science, a technique for estimating the height of a

building in an image is in progress. It could be estimated in a more detail surface temperature in the image by including a energy balance model, which would be part of the future work. In addition, SVF, an important factor in estimating the solar radiation, used images taken from roads, not pedestrian paths. As the value of SVF varies greatly depending on the point where it is photographed, it is difficult to represent the thermal comfort of pedestrians with images photographed on the roadway. However, since we can produce 360-degree panorama images at any point through the street view app, it is easier to construct spatial data than other models (ENVI-met, SOLWEIG, etc.) and can be easily accessed. Therefore, the MRT can be estimated through a 360-degree image anywhere a user prefer.

Although Based on the data from 7 measurements in Seoul, we confirmed the possibility for the proposed method. this has limitation only possible in clear-sky day. Thus it is difficult to apply in regions with cloudy weather. However when there is meteorological input data such as turbidity and atmospheric pressure, it can be used in all regions by using the method proposed in (Dervishi & Mahdavi, 2012; Matzarakis et al., 2010). Finally the meteorological data required to estimate MRT was used as AWS data. This cannot be reflected at all points location in Seoul. hence slight error may occur in the result of estimated MRT mapping the Seoul city. However, with the recent increase in the field of citizen science, This limitation can be developed using wide range and high-resolution citizen data in the future work

Chapter 5. Conclusion

This study focuses on (1) approach for calculating the MRT with shortwave, longwave radiation in street-level using publicly available GSV images; (2) investigating the impacts of street canyon geometries(street orientation) and morphologies (sky opening and obstructions by trees) on street-level solar radiation; (3) analyzed relationship between LST and MRT. Verifications of our developed method using field measurements in various regions(residential area, high-density building, park, open space) show that the clear-sky solar radiance of street canyons accurately capture the diurnal cycle in high-density environments($R^2 = 0.97$). Although differences between the observed longwave radiation and estimated longwave radiation were found by changing albedo with altitude of the sun, Calculation method using a simplified energy balance model, we estimated high accuracy as (R^2= 0.77). Additionally, we compared land surface temperature from Landsat 8 and result of MRT mapped using the method proposed and and investigate solar radiation under the effect of urban geometries

Generally sites with high LST and MRT were distributed in similar spaces, but low plants with low LST values as permeable layers showed high MRT values with high SVF (>0.95), and in compact low-rise density buildings with high LST values, The MRT value was low due to surrounding obstacles (BVF, TVF are around 0.4-0.6, 0.6-0.99). And the spatial variability of street-level MRT

is closely related to high tree cover. Lower MRT is received in north-south street orientation during daytime and high TVF. In particular shortwave radiation has a large impact on the shaded area in street-level. The developed method in this study to map the street-level MRT can be applied to cities with available coverage of GSV images. This method provides a low-cost and effective streetscape mapping approach for urban studies. Clear-sky street-level MRT can be derived for cities with basic meteorological measurements including Air temperature, Humidity while street-level MRT can be further calculated. The resulted maps of street-level solar radiation provide crucial datasets for studying the spatial and temporal variabilities of street-level MRT and understanding the interactions between solar radiation , human health in the street-level.

Bibliography

Aleksandrowicz, O., Zur, S., Lebendiger, Y., & Lerman, Y. (2020). Shade maps for prioritizing municipal microclimatic action in hot climates: Learning from Tel Aviv–Yafo. Sustainable Cities and Society, 53(September 2019), 101931. https://doi.org/10.1016/j.scs.2019.101931

Bogren, J., Gustavsson, T., Karlsson, M., & Postgård, U. (2000). The impact of screening on road surface temperature. Meteorological Applications, 7(2), 97–104. https://doi.org/10.1017/S135048270000150X

Bonamente, E., Rossi, F., Coccia, V., Pisello, A. L., Nicolini, A., Castellani, B., … Santamouris, M. (2013). An energy-balanced analytic model for urban heat canyons: comparison with experimental data. Advances in Building Energy Research, 7(2), 222–234. https://doi.org/10.1080/17512549.2013.865561

Cândido, R. L., Steinmetz-Wood, M., Morency, P., & Kestens, Y. (2018). Reassessing Urban Health Interventions: Back to the Future with Google Street View Time Machine. American Journal of Preventive Medicine, 55(5), 662–669. https://doi.org/10.1016/j.amepre.2018.04.047

Chen, L., Yu, B., Yang, F., & Mayer, H. (2016). Intra-urban differences of mean radiant temperature in different urban settings in Shanghai and implications for heat stress under heat waves: A GIS-based approach. Energy and Buildings, 130, 829–842. https://doi.org/10.1016/j.enbuild.2016.09.014

Chen, Y. C., Chen, C. Y., Matzarakis, A., Liu, J. K., & Lin, T. P. (2016). Modeling of mean radiant temperature based on comparison of airborne remote sensing data with surface measured data. Atmospheric Research, 174–175, 151–159. https://doi.org/10.1016/j.atmosres.2016.01.004

Chow, A., Fung, A. S., & Li, S. (2014). GIS modeling of solar

neighborhood potential at a fine spatiotemporal resolution. Buildings, 4(2), 195–206. https://doi.org/10.3390/buildings4020195

Cohen, S., Palatchi, Y., Palatchi, D. P., Shashua-Bar, L., Lukyanov, V., Yaakov, Y., ... Potchter, O. (2020). Mean radiant temperature in urban canyons from solar calculations, climate and surface properties – Theory, validation and 'Mr.T' software. Building and Environment, 178(May), 106927. https://doi.org/10.1016/j.buildenv.2020.106927

Doan, Q. Van, Kusaka, H., & Ho, Q. B. (2016). Impact of future urbanization on temperature and thermal comfort index in a developing tropical city: Ho Chi Minh City. Urban Climate, 17, 20–31. https://doi.org/10.1016/j.uclim.2016.04.003

Dousset, B., Gourmelon, F., Laaidi, K., Zeghnoun, A., Giraudet, E., Bretin, P., ... Vandentorren, S. (2011). Satellite monitoring of summer heat waves in the Paris metropolitan area. International Journal of Climatology, 31(2), 313–323. https://doi.org/10.1002/joc.2222

Eckstein, D., Künzel, V., Schäfer, L., & Winges, M. (2020). Global Climate Risk Index 2020. Retrieved from https://www.germanwatch.org/sites/germanwatch.org/files/20-2-01e Global Climate Risk Index 2020_14.pdf

Elwy, I., Ibrahim, Y., Fahmy, M., & Mahdy, M. (2018). Outdoor microclimatic validation for hybrid simulation workflow in hot arid climates against ENVI-met and field measurements. Energy Procedia, 153(November), 29–34. https://doi.org/10.1016/j.egypro.2018.10.009

Evola, G., Costanzo, V., Magrì, C., Margani, G., Marletta, L., & Naboni, E. (2020). A novel comprehensive workflow for modelling outdoor thermal comfort and energy demand in urban canyons: Results and critical issues. Energy and Buildings, 216, 109946. https://doi.org/10.1016/j.enbuild.2020.109946

Fröhlich Dominik and Matzarakis Andreas. (2013) Modeling of

changes in thermal bioclimate examples based on urban spaces in Freiburg, Germany. Theor Appl Climatol. 111: 547–558. http://doi.org/10.1007/s00704-012-0678-y

Gabriel, K. M. A., & Endlicher, W. R. (2011). Urban and rural mortality rates during heat waves in Berlin and Brandenburg, Germany. Environmental Pollution, 159(8–9), 2044–2050. https://doi.org/10.1016/j.envpol.2011.01.016

Gál, C. V., & Kántor, N. (2020). Modeling mean radiant temperature in outdoor spaces, A comparative numerical simulation and validation study. Urban Climate, 32(December 2019), 100571. https://doi.org/10.1016/j.uclim.2019.100571

Gomes, D. L., dos Reis, P. R. J., de Paiva, A. C., Silva, A. C., Braz, G., de Araújo, A. S., & Gattass, M. (2017). Semi-automatic methodology for augmented panorama development in industrial outdoor environments. Advances in Engineering Software, 114, 282–294. https://doi.org/10.1016/j.advengsoft.2017.07.012

Gong, F. Y., Zeng, Z. C., Ng, E., & Norford, L. K. (2019). Spatiotemporal patterns of street-level solar radiation estimated using Google Street View in a high-density urban environment. Building and Environment, 148(October 2018), 547–566. https://doi.org/10.1016/j.buildenv.2018.10.025

Gong, F. Y., Zeng, Z. C., Zhang, F., Li, X., Ng, E., & Norford, L. K. (2018). Mapping sky, tree, and building view factors of street canyons in a high-density urban environment. Building and Environment, 134(March), 155–167. https://doi.org/10.1016/j.buildenv.2018.02.042

He, Y., Wetterhall, F., Cloke, H. L., Pappenberger, F., Wilson, M., & Freer, J. (2009). Tracking the uncertainty in flood alerts driven by grand. Meteorological Applications, 101(February), 91–101. https://doi.org/10.1002/met

Indices, T. (2017). RayManManual.pdf.

Jakubiec, J. A., & Reinhart, C. F. (2013). A method for predicting city-wide electricity gains from photovoltaic panels based on

LiDAR and GIS data combined with hourly Daysim simulations. Solar Energy, 93, 127–143. https://doi.org/10.1016/j.solener.2013.03.022

Jamei, E., & Rajagopalan, P. (2017). Urban development and pedestrian thermal comfort in Melbourne. Solar Energy, 144, 681–698. https://doi.org/10.1016/j.solener.2017.01.023

Jänicke, B., Meier, F., Lindberg, F., Schubert, S., & Scherer, D. (2016). Towards city-wide, building-resolving analysis of mean radiant temperature. Urban Climate, 15, 83–98. https://doi.org/10.1016/j.uclim.2015.11.003

Jonsson, P., Eliasson, I., Holmer, B., & Grimmond, C. S. B. (2006). Longwave incoming radiation in the Tropics: Results from field work in three African cities. Theoretical and Applied Climatology, 85(3–4), 185–201. https://doi.org/10.1007/s00704-005-0178-4

Krüger, E., Drach, P., Emmanuel, R., & Corbella, O. (2013). Urban heat island and differences in outdoor comfort levels in Glasgow, UK. Theoretical and Applied Climatology, Vol. 112, pp. 127–141. https://doi.org/10.1007/s00704-012-0724-9

Li, X., Ratti, C., & Seiferling, I. (2018). Quantifying the shade provision of street trees in urban landscape: A case study in Boston, USA, using Google Street View. Landscape and Urban Planning, 169(August 2017), 81–91. https://doi.org/10.1016/j.landurbplan.2017.08.011

Liang, J., Gong, J., Zhang, J., Li, Y., Wu, D., & Zhang, G. (2020). GSV2SVF-an interactive GIS tool for sky, tree and building view factor estimation from street view photographs. Building and Environment, 168(October 2019). https://doi.org/10.1016/j.buildenv.2019.106475

Lindberg, F., Holmer, B., & Thorsson, S. (2008). SOLWEIG 1.0 - Modelling spatial variations of 3D radiant fluxes and mean radiant temperature in complex urban settings. International Journal of Biometeorology, 52(7), 697–713. https://doi.org/10.1007/s00484-008-0162-7

Lindberg, F., Onomura, S., & Grimmond, C. S. B. (2016). Influence of ground surface characteristics on the mean radiant temperature in urban areas. International Journal of Biometeorology, 60(9), 1439–1452. https://doi.org/10.1007/s00484-016-1135-x

Manavvi, S., & Rajasekar, E. (2020). Estimating outdoor mean radiant temperature in a humid subtropical climate. Building and Environment, 171(June 2019), 106658. https://doi.org/10.1016/j.buildenv.2020.106658

Middel, A., & Krayenhoff, E. S. (2019). Micrometeorological determinants of pedestrian thermal exposure during record-breaking heat in Tempe, Arizona: Introducing the MaRTy observational platform. Science of the Total Environment, 687, 137–151. https://doi.org/10.1016/j.scitotenv.2019.06.085

naboni, emanuele, meloni, marco, makey, chris, & kaempf, jerome. (2020). The Simulation of Mean Radiant Temperature in Outdoor Conditions: A review of Software Tools Capabilities. Proceedings of Building Simulation 2019: 16th Conference of IBPSA, 16, 3234–3241. https://doi.org/10.26868/25222708.2019.210301

Oswald, S. M., Revesz, M., Trimmel, H., Weihs, P., Zamini, S., Schneider, A., … Lindberg, F. (2018). Coupling of urban energy balance model with 3-D radiation model to derive human thermal (dis)comfort. International Journal of Biometeorology, 711–722. https://doi.org/10.1007/s00484-018-1642-z

Paper, C., & Kong, H. (2016). a Gis-Based Assessment Method for Mean Radiant Temperature 2 in Dense Urban Areas . (April). Retrieved from http://web.mit.edu/tito_/www/Publications/SimBuild2012_MeanRadiantTemperature_Huang.pdf

Park, C. Y., Lee, D. K., Krayenhoff, E. S., Heo, H. K., Ahn, S., Asawa, T., … Kim, H. G. (2018). A multilayer mean radiant

temperature model for pedestrians in a street canyon with trees. Building and Environment, 141(March), 298–309. https://doi.org/10.1016/j.buildenv.2018.05.058

Perini, K., Chokhachian, A., Dong, S., & Auer, T. (2017). Modeling and simulating urban outdoor comfort: Coupling ENVI-Met and TRNSYS by grasshopper. Energy and Buildings, 152, 373–384. https://doi.org/10.1016/j.enbuild.2017.07.061

Reda, I., & Nrel, A. A. (2005). Solar Position Algorithm for Solar Radiation Applications (Revised). National Renewable Energy Laboratory Nrel/Tp-560-34302, (January), 1–56. https://doi.org/10.2172/15003974

Robinson, D., Haldi, F., Kämpf, J., Leroux, P., Perez, D., Rasheed, A., & Wilke, U. (2009). Citysim: Comprehensive micro-simulation of resource flows for sustainable urban planning. IBPSA 2009 - International Building Performance Simulation Association 2009, (July), 1083–1090.

Roudsari, M. S., & Pak, M. (2013). Ladybug: A parametric environmental plugin for grasshopper to help designers create an environmentally-conscious design. Proceedings of BS 2013: 13th Conference of the International Building Performance Simulation Association, (January 2013), 3128–3135.

Ryu, Y. H., Baik, J. J., & Lee, S. H. (2011). A new single-layer urban canopy model for use in mesoscale atmospheric models. Journal of Applied Meteorology and Climatology, 50(9), 1773–1794. https://doi.org/10.1175/2011JAMC2665.1

The Mathworks MATLAB. (2018). Introducing Deep Learning with MATLAB: “What is Deep Learning?” Retrieved from https://www.mathworks.com/content/dam/mathworks/ebook/gated/80879v00_Deep_Learning_ebook.pdf

Thorsson, S., Rayner, D., Lindberg, F., Monteiro, A., Katzschner, L., Lau, K. K. L., … Holmer, B. (2017). Present and projected future mean radiant temperature for three European cities. International Journal of Biometeorology, 61(9), 1531–1543.

https://doi.org/10.1007/s00484-017-1332-2
Thorsson, S., Rocklov. J., Konarska. J, Lindberg. F., Holmer. B., Dousset. B. Rayner. David (2014) Mean radiant temperature – A predictor of heat related mortality. Urban Climate, 10,332-345. https://doi.org/10.1016/j.uclim.2014.01.004
Tran Thi Van, Ha Duong Xuan Bao, & Nguyen Thi Tuyet Mai. (2017). Urban thermal environment and heat island in Ho Chi Minh City , Vietnam from remote sensing data. Preprints, (January), 1–12. https://doi.org/10.20944/preprints201701.0129.v1
Tran, D. N., Doan, V. Q., Nguyen, V. T., Khan, A., Thai, P. K., Cunrui, H., … Phung, D. (2020). Spatial patterns of health vulnerability to heatwaves in Vietnam. International Journal of Biometeorology, 64(5), 863–872. https://doi.org/10.1007/s00484-020-01876-2
Yu, B., Liu, H., Wu, J., & Lin, W. M. (2009). Investigating impacts of urban morphology on spatio-temporal variations of solar radiation with airborne LIDAR data and a solar flux model: A case study of downtown Houston. International Journal of Remote Sensing, 30(17), 4359–4385. https://doi.org/10.1080/01431160802555846

Abstract in Korean

도시개발로 인해 보행자의 에너지 균형을 변화시키며 도시공간의 열쾌적성이 악화되는 등 열 환경문제가 발생하고 있다. 선행연구에서는 도시 공간 내 열 쾌적성을 정량적으로 평가하기 위해 인간의 가장 중요한 생체 기상 변수 중 하나인 평균복사온도를 산정하는 연구가 진행되고 있다. 하지만 산정식이 복잡하거나, 넓은 범위에서의 공간 데이터 취득이 어렵기 때문에, 커뮤니티 단위에서 고해상도의 평균복사온도를 추정하는 것은 어렵다. 따라서 본 연구에서는 구글스트릿뷰 이미지를 사용하여 도시 거리 협곡내 평균복사 온도를 추정하는 방법을 제시하고, 도시 스케일에서 도시열섬 분석을 위해 많은 연구가 진행된 지표면 온도와 평균복사온도간 관계를 공간패턴 측면에서 분석하였다. 우선 평균복사온도 추정식에 큰 영향을 미치는 천공률은 파노라마 이미지를 바탕으로 딥러닝을 활용하여 도시 요인별(건물, 나무, 하늘 등)분류하고, 어안렌즈 이미지로 변환하여 도출하였다. 또한 어안렌즈 이미지를 중심으로 태양경로 알고리즘을 활용하여 시간별 그림자의 유무를 판단하였다. 마지막으로 기후요인, 시간, 위치 등 데이터를 활용하여 장파, 단파 복사를 도출하여 평균복사온도를 산정하였다.

제안된 평균복사온도 추정 방법과 실측간 비교(7 곳) 결과 단파, 장파 값의 R^2 값이 각각 0.97, 0.77로 나타났다. 다른 모델과 비교한 결과, 높은 정확도를 확인할 수 있으며 복잡한 도시 환경에서의 활용가능성을 확인할 수 있다. 도시규모에서 지표면온도, 평균복사온도를 공간패턴 측면에서 비교한 결과 천공률, 빌딩 뷰팩터가 각각 0.6~1.0, 0.35−0.5인 오픈스페이스 혹은 저층 밀집지역에서 높은

평균복사온도(>59.4° C)를 보였다. 반면 높은 빌딩이 밀집된 지역의 경우(빌딩 뷰팩터 :0.4-0.6, 나무 뷰팩터 0.6-0.9) 낮은 평균복사온도(<47.6° C)를 보였다. 특히 거리의 방향이 동-서 인 경우에는 천공률이 0.3-0.55 일지라도 높은 평균복사온도를 확인할 수 있었다. 추가적으로 평균복사온도와 지표면 온도간 비교결과 전반적으로 높은 온도 값을 가진 공간이 유사하였으나, 저층 고밀도 건물 지역 혹은 초지 지역에서 상반된 결과를 확인할 수 있었다.

본 연구에서는 도시스케일에서 높은 해상도로 평균복사온도를 추정하는 방법을 딥러닝을 활용하여 제시하였으며, 지표면 온도와 공간패턴별 분석을 통해 실제 보행자가 체감하는 열 환경을 개선하기 위한 방안을 제시할 수 있는 기초자료를 제공하였다. 이는 도시 열 환경을 고려한 지속가능한 도시 공간 설계 및 환경 계획 측면에서 활용될 수 있으며, 특히 공간데이터 취득이 어려운 곳에서의 높은 활용성을 기대해 볼 수 있다.

주요어: 도시열섬, 평균복사온도, 열 쾌적성, 딥러닝, 구글 스트릿뷰,

학번: 2019-20217

Appendix

Appendix 1 Validation of solar radiation in korea. (Appendix A.1) show that the clear-sky solar radiance of street canyons for a day in high-density and Low building environments. Yellow, blue, green, black line indicate same as (section 3.1.1).

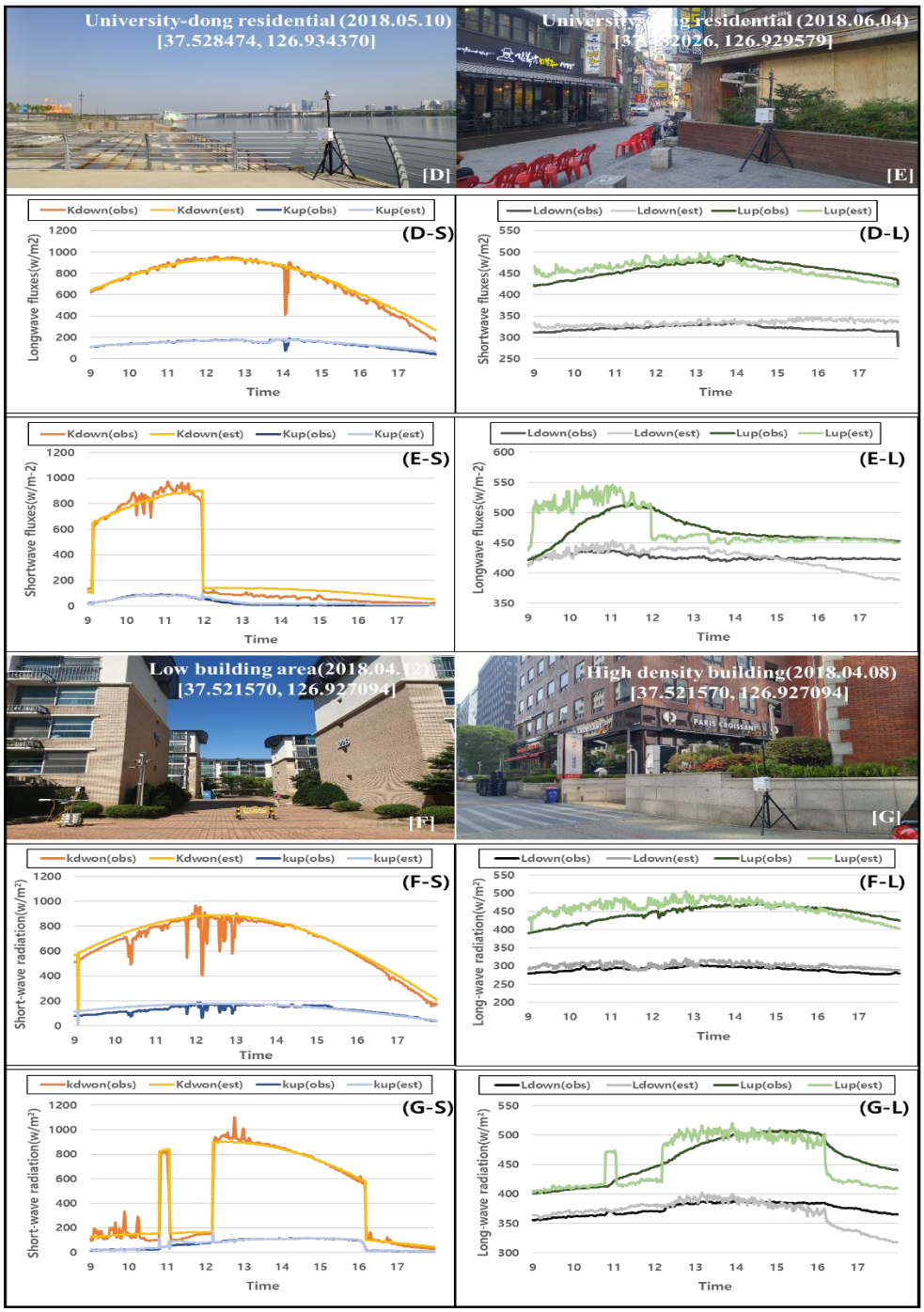

Appendix 2 same as Appendix. 1

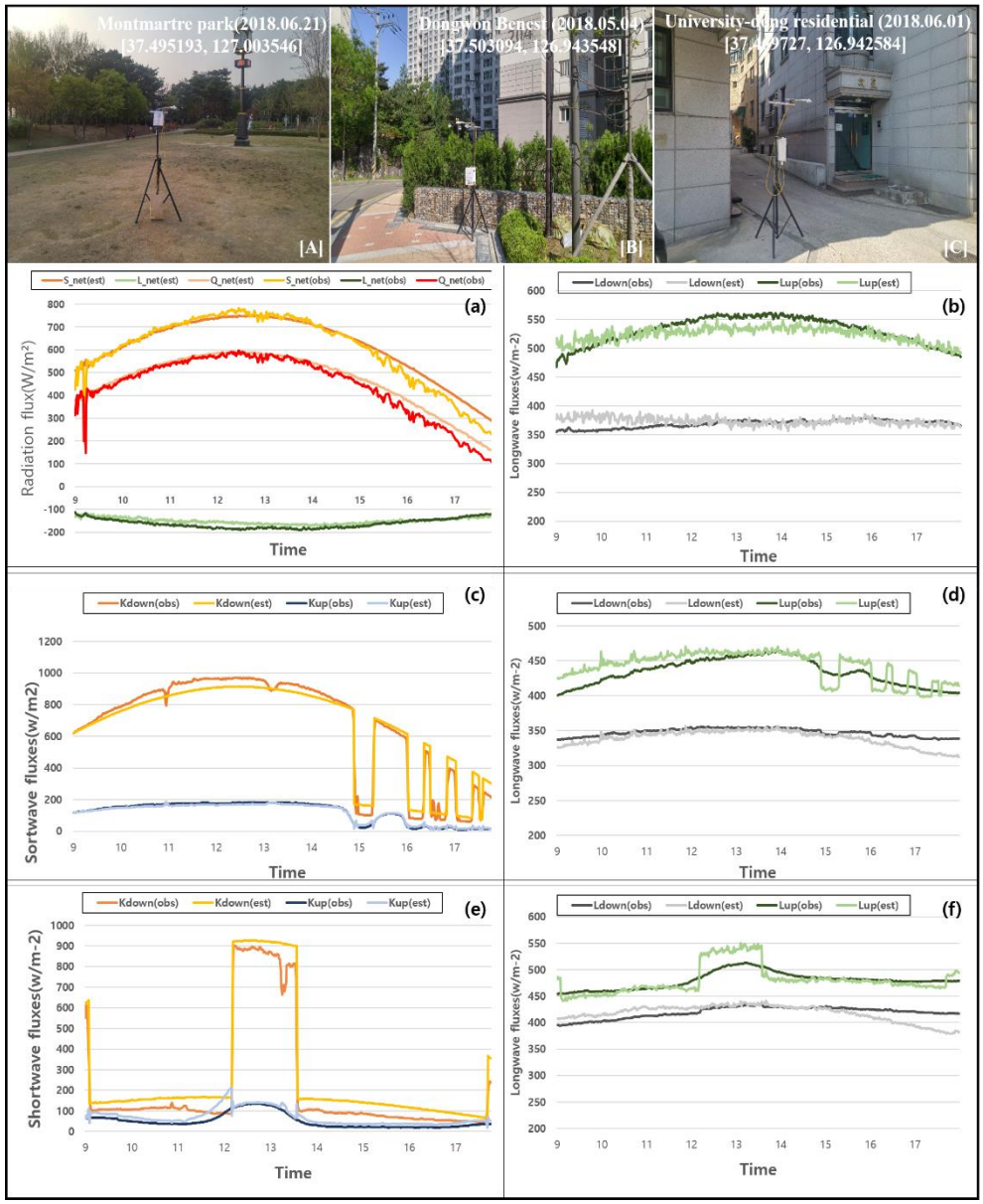

Appendix 3 Training a neural network for deep learning. Run the trained neural network on a set of tests not used to train the neural network and predict the image labels